Scientia Iranica, Vol. 12, No. 4, pp 379–391

SCIENTIA
IRANICA

A New Approach to Investigate Unsteady Aerodynamic Phenomena

M.R. Soltani* **and A.R. Davari**[1]

A new approach, based on a Generalized Regression Neural Network (GRNN), has been proposed to predict the unsteady forces and moments of two different models; a 70° swept delta wing in subsonic incompressible flow and a standard fighter model (SDM) in a compressible flow regime, both undergoing sinusoidal pitching motion. Extensive wind tunnel results were used for training the network and verification of the values predicted by this approach. GRNN was trained by the aforementioned experimental data and, subsequently, was used as a prediction tool to determine the unsteady longitudinal forces and moment of the two models under various conditions. Further, it was applied to extend the experimental data beyond the conditions tested in the tunnel. The results are in a good agreement with the experimental findings. This indicates that the present prediction and optimization tool provides sufficient accuracy with a modest amount of experimental data.

INTRODUCTION

Classic experimental methods have been popular for many years and have formed the basis of the conventional wind tunnel testing procedures used today. The defining feature of classic testing methods is the Error Control Strategy that requires each independent variable to be changed one at a time, while holding all other variables constant. The authors, however, suggest a new approach to aerodynamic prediction problems. The approach is based on creating an experimental data bank. An intelligent block uses this data to extract a reasonable trend and extend the results to any other cases out of this data bank. This intelligent block is called an Artificial Neural Network.

Artificial neural networks are relatively crude electronic models based on the neural structure of the brain. The brain basically learns from experience. It is natural that some problems beyond the scope of current computers are indeed solvable by small energy efficient packages, called brain modeling. This brain modeling promises a less technical way of developing machine solutions.

Recently, neural networks have been applied to a wide range of aerospace problems, e.g., the aerodynamic performance optimization of a rotor blade design [1], prediction of measured data to enable identification of instrument system degradation [2], etc. Most of the previous applications of neural networks in aerospace industries have been concentrated on several aerospace problems, such as high performance aircraft autopilots, flight path simulations, aircraft control systems, component simulations and structural fault detectors, etc. While the aforementioned subjects are important, finding an alternative method for difficult, expensive and time consuming wind tunnel tests or computational methods is necessary for predicting the behavior of present and future flying vehicles.

The neural network in fluid mechanics is still a new concept. Little work has been done in this field. Faller and Schreck [3] used neural networks to predict the real-time three-dimensional unsteady separated flowfields and aerodynamic coefficients of a pitching wing. This work was restricted to a wing alone and a whole aircraft or missile configuration has not been considered. Lo and Zhao [4] combined the nonlinear neural network methods with conventional linear regression techniques in wind tunnel force mea-

*. *Corresponding Author, Department of Aerospace Engineering, Sharif University of Technology, Tehran, I.R. Iran.*

1. *Department of Aerospace Engineering, Sharif University of Technology, Tehran, I.R. Iran.*

surements. However, their study was only for static cases. Berdahl [5] recently proposed a new application of neural networks in the observation of shock waves in a supersonic channel flow. Though many attempts have been made to apply the neural network concept to aerospace problems, none has been reported or being used as a prediction tool for estimating the aerodynamic forces and moments for a whole aircraft or missile in an unsteady flow field.

In addition, tight and lower program budgets, as well as aggressive schedules, will no longer allow either the extensive wind tunnel test programs implemented in the past or a thorough numerical investigation to study and predict the aerodynamic behavior of flying vehicles, especially during unsteady maneuvers. Thus, the introduction of an alternative tool, enabling one to foresee unsteady aerodynamic behavior, will be of great importance.

This paper addresses a novel approach to predict the unsteady aerodynamic behavior of flying vehicles. The method is based on neural networks and is sufficiently fast, simple and accurate enough to predict aerodynamic variables. Extensive wind tunnel tests have been conducted on two different models oscillating in pitch in different flow conditions. The first model was a 70° swept delta wing tested in subsonic incompressible flow.

The second model was a typical fighter called SDM, which has been tested in several research centers all over the world. In these investigations, the second model was tested in compressible flow and at moderate to high oscillation frequencies. Although numerous results on SDM have been published [6-9], there is still insufficient information about its aerodynamic behavior, especially in high subsonic and supersonic regimes at high frequencies.

The goal was to gain physical insight into the unsteady flow phenomena using two different oscillating models and, further, to introduce a new prediction tool, based on a neural network, to determine the unsteady longitudinal aerodynamic forces and moment of the two models. The experimental data have been partly used for training the network and the rest have been used to check the ability of the network as a prediction tool. In addition, the effects on these models of different parameters and flow conditions on an unsteady flowfield have been studied.

The acquired wind tunnel data were used to train a GRNN network. The scheme, once proved to give correct results for various conditions tested in the tunnel, was extended to include other conditions that had not been tested in the tunnel. Furthermore, the network was used to predict the normal force and pitching moment of both models beyond the conditions used for training the system. The results show an interesting relationship between reduced frequency, oscillation amplitude and the hysteresis loops observed in the normal force and pitching moment data.

GENERALIZED REGRESSION NEURAL NETWORK (GRNN)

Artificial neural networks are a wide class of flexible nonlinear regression and discriminate models, data reduction models and nonlinear dynamic systems. The neural networks often consist of a large number of neurons, which are simply linear or nonlinear computing elements, interconnected in some complex ways and normally structured into layers.

The General Regression Neural Network (GRNN) was first introduced by Donald Specht in 1991 [10] and its topology is shown in Figure 1. The GRNN architecture consists of an input layer followed by three computational layers: Pattern, summation and output. When an input pattern is presented at the input layer, the pattern layer units compute the Euclidean distance between its weight vector and the input vector. This distance is then transformed by the unit's activation function, which are exponential (Gaussian) functions.

In a prediction problem such as aerodynamic modeling, the number of neurons in the input layer is equal to the number of input variables, and the number of neurons in the output layer is the same as the number of predicted variables. Selection of the rest of the architecture in the network, in terms of the number of neurons in the hidden layer, the learning rate, etc., is not an exact science and one has to resort to trial and error methods to find a suitable network structure for a given problem.

Consider the dependent vectors Y and X. These

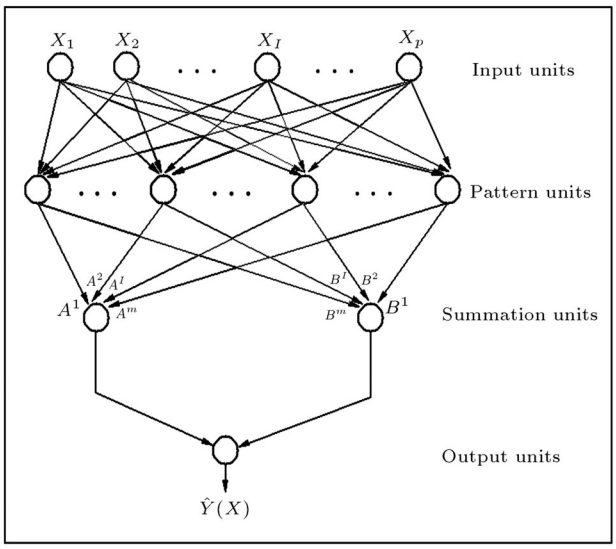

Figure 1. The generalized regression neural network.

variables are known as the system's output and input, respectively. The regression of a dependent variable, Y, on an independent variable, X, is the computation of the most probable value of Y for each value of X by taking a finite number of X measurements. For this reason, it is usually necessary to assume some functions with unknown parameter a_i. The values of these parameters are chosen to provide the best fit to the measured data. The approach presented here uses a method that does not require a specific functional form. It allows the appropriate form to be expressed as a Probability Density Function (PDF), which is determined empirically from the observed data. Thus, the method is not limited and does not require pre-knowledge of any particular form.

Assume that $f(x,y)$ represents the known joint continuous probability density function of the vector random variable, x, and a scalar random variable, y. Let X be the particular measured value of the random variable, x. The conditional mean of y for a given X (also called the regression of y on X) is given by:

$$E(y|X) = \frac{\int_{-\infty}^{\infty} y f(X,y)dy}{\int_{-\infty}^{\infty} f(X,y)dy}. \tag{1}$$

When the density function $f(x,y)$ is not known, it is usually estimated from a sample of observations of x and y. For a non-parametric estimate of $f(x,y)$, Parzen [11] proposed a class of consistent estimators for one-dimensional cases. Further estimators for multidimensional cases were proposed by Cacoullos [12]. These estimators are good choices for estimating the probability density function, $f(x,y)$, if it can be assumed that the density is continuous and that the first partial derivatives of the function evaluated at any x are sufficiently small. The probability estimator, $\hat{f}(X,Y)$, is based on the sample values X^i and Y^i of the random variables, x and y, and is expressed as:

$$\hat{f}(X,Y) = \frac{1}{(2\pi)^{(p-1)/2}\sigma^{(p+1)}} \cdot \frac{1}{n}\sum_{i=1}^{n} \exp\left[-\frac{(X-X^i)^2}{2\sigma^2}\right] \exp\left[-\frac{(Y-Y^i)^2}{2\sigma^2}\right], \tag{2}$$

where n is the number of sample observations, p is the dimension of the vector variable, x, and σ is the correlation parameter, which will be explained later in this section. Substituting the joint probability estimate, $\hat{f}$, from Equation 2 into the conditional mean (Equation 1) the desired conditional mean of y for a given X will be obtained. In particular, combining Equations 1 and 2 and interchanging the orders of integration and summation results in the desired conditional mean, $\hat{Y}(X)$:

$$\hat{Y}(X) = \frac{\sum_{i=1}^{n} \exp\left[-\frac{(X-X^i)^2}{2\sigma^2}\right] \int_{-\infty}^{\infty} y \times \exp\left[-\frac{(y-Y^i)^2}{2\sigma^2}\right] dy}{\sum_{i=1}^{n} \exp\left[-\frac{(X-X^i)^2}{2\sigma^2}\right] \int_{-\infty}^{\infty} \exp\left[-\frac{(y-Y^i)^2}{2\sigma^2}\right] dy}. \tag{3}$$

Defining the scalar function, D_i^2, as: $D_i^2 = (X - X^i)^T(X - X^i)$ and performing the integration yields the following expression:

$$\hat{Y}(X) = \frac{\sum_{i=1}^{n} Y^i \exp(-\frac{D_i^2}{2\sigma^2})}{\sum_{i=1}^{n} \exp(-\frac{D_i^2}{2\sigma^2})}. \tag{4}$$

Parzen and Cacoullos [11,12] have shown that the probability estimator, $\hat{f}(x,y)$, in the form of Equation 2 is a consistent estimator, i.e., it asymptotically converges to the underlying probability density function, $f(x,y)$, at all points, (x,y). However, the density function, $f(x,y)$, is continuous and $\sigma = \sigma(n)$ is a decreasing function of n, such that:

$$\lim_{n\to\infty} \sigma(n) = 0,$$

and:

$$\lim_{n\to\infty} n\sigma^n(n) = \infty.$$

The topology of a GRNN shown in Figure 1 consists of four layers; the input layer, the hidden layer, the summation layer and the output layer. The input layer passes the input vector variable, X, to all the units in the hidden layer, which consists of all the training samples, $X_1, \cdots, X_n$. Further, the scalar function, D_i^2, between the unknown pattern and the training sample is calculated and passed through the kernel function. As illustrated in Figure 1, the summation layer has two units; A and B. While unit A computes the summation of $\exp[-D_i^2/2\sigma^2]$, multiplied by the Y_i associated with X_i, unit B computes the summation of $\exp[-D_i^2/2\sigma^2]$. Finally, the output unit divides A by B to provide the prediction result as:

$$\hat{Y}(X) = \frac{\sum_{i=1}^{n} A^i \exp\left[-\frac{D_i^2}{2\sigma^2}\right]}{\sum_{i=1}^{n} B^i \exp\left[-\frac{D_i^2}{2\sigma^2}\right]}, \tag{5}$$

with $A^i(k)$ and $B^i(k)$ defined as:

$$A^i(k) = A^i(k-1) + Y^i,$$

$$B^i(k) = B^i(k-1) + 1,$$

where $A^i(k)$ and $B^i(k)$ are the values of the coefficients for cluster i after k observations and are the summation of the Y values and the number of samples assigned to cluster i, respectively [10].

The correlation or smoothing parameter, σ, defined in Equation 4, is one of the most important parameters in a GRNN structure. If this parameter is made large, the estimated density is forced to be smooth. On the other hand, the smaller value of σ allows the estimated density function to assume a non-Gaussian shape. However, for an accurate prediction, σ must be optimized [13].

Suppose that in a GRNN network there are k predicted values of $(X^i, Y^i)_{i=1,\cdots,k}$, which are inputs and outputs, respectively. The optimum value of σ minimizes the mean error [14], defined by:

$$E_{\text{mean}} = \frac{\sum_{i=1}^{k} \left| Y_e(X^i) - Y^i \right|}{k},$$

where $Y_e(X^i)$ and Y^i are real and predicted values, respectively. A useful method for selecting σ is called the holdout method. This method consists of removing one sample at a time and constructing the new network based on all other samples, which will be used to estimate Y for the removed sample. By repeating this process for each sample and storing each estimate, the mean squared error can be measured between the actual and the predicted samples. The value of σ that gives the smallest error is an optimum one and should be used in the prediction steps [10].

In the present investigation, two models, a 70° swept delta wing model and a fighter model, both undergoing sinusoidal pitching motions in subsonic flow, were considered. Various experiments at different conditions have been carried out. For the delta wing model, the pitching frequency and the instantaneous angles of attack were used as the training data for GRNN, while the velocity, sideslip angle and Reynolds number were constant. However, the experiments were conducted at various Reynolds numbers, reduced frequencies and sideslip angles. For the SDM model, oscillation frequency, oscillation amplitude and Mach number were fixed and the network has been trained with various mean and instantaneous angles of attack. The experimental data for this model included the effects of reduced frequencies, mean angles of attack and Mach numbers for both sinusoidal pitching and plunging motions.

The system outputs for the delta wing model were normal, as well as the drag forces and the pitching moment coefficients, (C_N, C_D and C_m). However, for the SDM model, the outputs were normal force and pitching moment coefficients only (C_N and C_m). This is because, for the delta wing model, forces and moments at various conditions were measured using a six-component internal strain gauge balance, while the balance used for the SDM model was a five-component type, i.e., the drag force was excluded.

Two types of output from the GRNN were considered. The first type was the results of interpolation, where the network was programmed to predict the aerodynamic force and moment at some conditions between the trained data. The second type, extrapolation, dealt with the conditions out of range of the data used for training the network. The results were compared with the experimental data. The comparisons show remarkable agreement between the experiments and GRNN outputs.

MODELS AND EXPERIMENTAL APPARATUS

Two different models have been used for these investigations. The first model was a simple flat plate delta wing with a 70° leading edge sweep and a 38.1 cm span at the trailing edge. A schematic view of this model is shown in Figure 2a. The second model was a standard model used in various dynamic tests all over the world [6-9]. It is a simplified version of the F-16 aircraft with air inlet and ventral fins and is known as SDM (Figure 2b).

The 70° delta wing model has been tested in the subsonic wind tunnel of the Ohio State University [15]. It is an indraft, open circuit tunnel which exhausts to the atmosphere. It has a test section of approximately $1.5 \times 0.9 \times 2.4$ m^3 and operates at speeds from 0 to 67 m/sec at the Reynolds numbers of up to 4.3×10^6 per

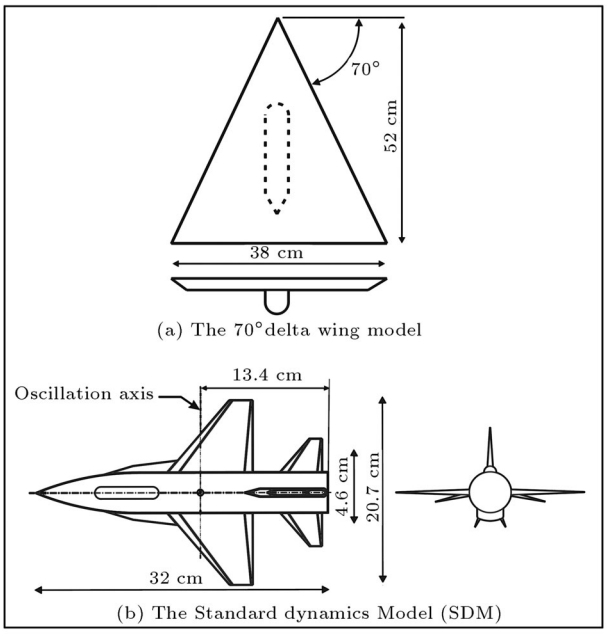

Figure 2. Models used for the present investigations.

meter. The model was sinusoidally oscillated in pitch from a 0° to 55° angle of attack at reduced frequencies ranging from 0.015 to 0.089. The sideslip angle was also varied between 0° and 15°.

The standard dynamic model, SDM, was tested in the transonic wind tunnel of Qhadr Research Center, Tehran. It is a continuous open circuit tunnel with test section dimensions of $60 \times 60 \times 120$ cm^3. The test section Mach number varies from 0.4 to 2.2, via the engine RPM and different nozzle settings.

Static, direct and cross coupling derivatives in pitch and plunge modes at various frequencies, Mach numbers and mean angles of attack were measured on the SDM. Static and oscillatory data were taken at the Mach numbers of 0.4, 0.6 and 1.5, which correspond to the Reynolds numbers of 0.84, 1.26 and 3.15×10^7 per meter, respectively. The mean angle of attack ranged from 0° to 15°. The oscillatory data were taken at oscillation amplitudes of ±1 and ±5 degrees and frequencies of 1.25, 2.77 and 6.00 Hz, which correspond to the reduced frequencies ranging from $k = 5.9 \times 10^{-4}$ to 1.0×10^{-2}.

The oscillation systems for both models are nearly the same. The system for testing the 70° delta wing model uses a belt and pulley arrangement to reduce the motor R.P.M. to speeds from zero to 2.3 Hz. The desired motion is produced by a cam. This cam generates a sinusoidal oscillation of the model inside the tunnel during the pitching motion. The system for testing the SDM uses a crankshaft to convert the circular motion of the motor to reciprocal motion, which is transferred to the model by means of rods. This system can oscillate the model with frequencies from 1.00 to 8.00 Hz.

The dynamic oscillatory data presented in this paper for both models are an average of several cycles at a sample rate based on the reduced frequency. Various data acquisition rates were tested to find the best combination, which would provide as many cycles of quality data as possible. Raw data were then digitally filtered using a low-pass filtering routine. During the filtering process, cut off and transition frequencies were varied until the deviation between the original and the filtered ones was at a minimum.

RESULTS AND DISCUSSION

In this section, the major predicted results and findings of the GRNN, along with the wind tunnel verification tests, are discussed. It is, however, beyond the scope of this paper to present all of the wind tunnel data, as well as the predicted ones. Only the data that support conclusions or are of particular interest are given. The main emphasis is on the dynamic normal force data, even though the pitching moment measurements were also included.

Figure 3 compares the measured static variation of the lift coefficient with an angle of attack for the delta wing model, with theory and other experiments [16]. For small incidences, the experimental data compare well with the predicted potential lift. As the incidence is increased, the measured lift data deviate from that predicted by the potential theory. The deviation is due to the additional lift produced by the leading edge vortices, which is not accounted for in the theory.

Good agreement is achieved when the present results are compared with Polhamus's method [17] for angles of attack below 28°. Large deviations between the experimental and theoretical values above an incidence of 28° are caused by the bursting phenomenon [18], which was not considered in Polhamus's method. Figure 3 has been presented to show the accuracy of our experimental setup. There were no dynamic data on a 70° delta wing under the same conditions considered here, hence, only the static data on this model have been compared with other experimental and theoretical findings.

As stated previously, the delta wing model was oscillated in pitch at various reduced frequencies, Reynolds numbers, sideslip angles and angles of attack up to 55°. Both static and dynamic force and moment data were measured using a six-component internal strain gauge balance. The dynamic data at various reduced frequencies were used to train the GRNN. Once the optimum σ for the ranges of the variables used to train the system, such as reduced frequencies, mean angles of attack, etc., was determined, the network output for the cases beyond the training data could be easily obtained. It should be noted that the optimum σ for each situation was determined for the given ranges of variables that were used as the training data.

Figure 4 shows the effects of σ on the mean error

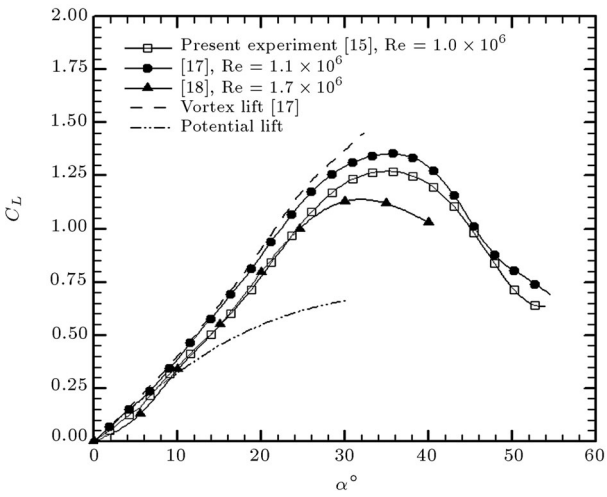

Figure 3. Variations of the static lift coefficient with angle of attack for the 70° delta wing model.

of the predicted data. It can be seen that for σ between 0.02 and 0.04, the mean error is minimum. For σ greater than 0.2, the mean error increases drastically. Further, for σ less than 0.02, the magnitude of the error increases slightly from its minimum value. Hence, the optimum value of σ for this case is between 0.02 and 0.04. The values of σ in this range give the best results for a 70° delta wing model at the ranges of the reduced frequencies studied in the present investigation. For this model, throughout the paper, a value of $\sigma = 0.02$ has been used to train the network.

Figure 5 shows the effect of σ on predicting the pitching moment coefficient for the reduced frequency of 0.015. Note that as σ decreases from 0.5 to 0.02, the differences between the predicted and measured data reduce continuously. For $\sigma = 0.02$, the predicted data compare well with the experimental results. This value of σ is within the values that give minimum error, as shown in Figure 4.

Figure 6 shows variations of the normal force, drag force and pitching moment coefficients with angle of attack for two different reduced frequencies; $k = 0.015$ and 0.048 [15]. The experimental data for both reduced frequencies are compared with the GRNN predicted data. The predicted data for each case is the result of either extrapolation or interpolation of the experimental data. Thus, for each case presented in Figures 6a and 6b, the GRNN has been trained such that its output is either interpolating or extrapolating the experimental data. For example, the GRNN was trained using the experimental variations of C_N, C_D and C_m with the angle of attack for the reduced

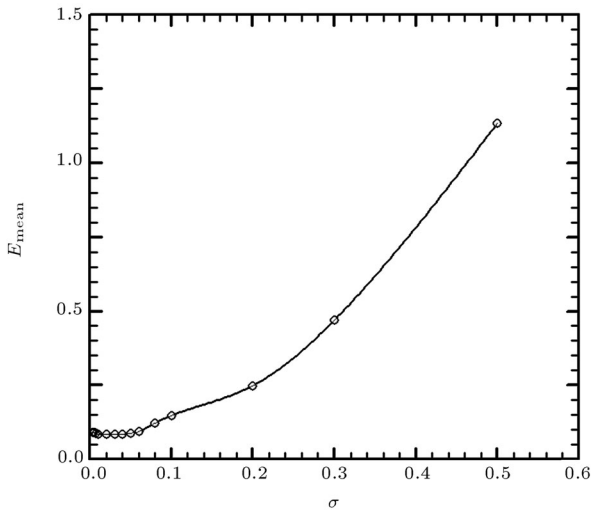

Figure 4. Effects of σ on the mean error prediction for the 70° delta wing model.

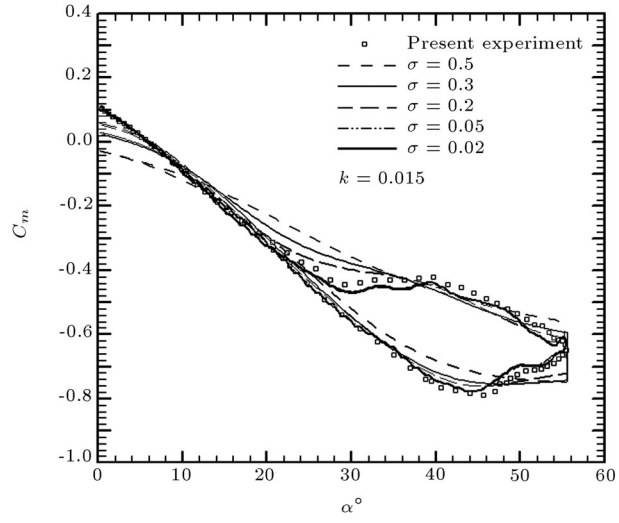

Figure 5. Effects of σ on prediction of the pitching moment coefficient for the 70° delta wing model.

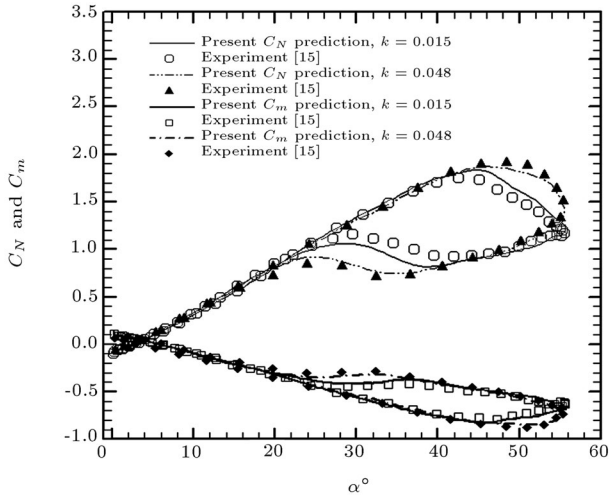

Figure 6a. Normal force and pitching moment coefficients predicted by the GRNN for the 70° delta wing model.

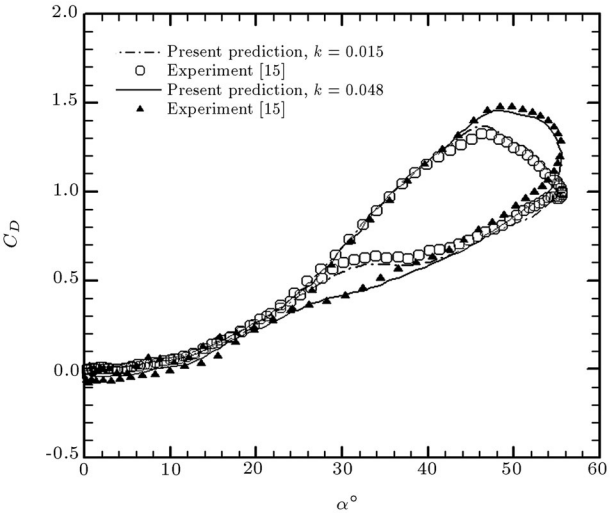

Figure 6b. Drag coefficients predicted by the GRNN for the 70° delta wing model.

frequencies of $k = 0.034$, 0.048 and 0.089, while its output is for $k = 0.015$, that is extrapolating the experimental data. For other reduced frequencies shown in this figure, the trained experimental data were for reduced frequencies of $k = 0.015$, 0.034 and 0.089 and the output is for $k = 0.048$, which is interpolating the experimental results. It should be noted that the least experimental data needed to train the network are three sets, i.e. three different reduced frequencies for this particular case.

Therefore, for the extrapolation case, the experimental data for the reduced frequencies of 0.034, 0.048 and 0.089 were used as training data, while for the interpolation one, the experimental data for $k = 0.015$, 0.034 and 0.048 were selected. If the experimental data for more ranges of reduced frequencies were available, there would be no need to train the network twice; once for interpolation and once for extrapolation. However, to the author's knowledge, no experimental data for a pitching delta wing under similar conditions as described in [15], i.e., Reynolds number, Mach number and angle of attack ranges, are available to be used as the training data, hence, it was necessary to train the network twice and predict the data for each case individually.

As can be seen, the experimental and predicted data are in good agreement. For both reduced frequencies shown in Figure 6, the error between the experimental and predicted values is almost zero, up to the stall region near the angle of attack of about 40° to 45°. Beyond this range, some discrepancies between the predicted and experimental data are observed, which are caused by the changes in the flowfield. This phenomenon is due to the delay in the flow separation and re-attachment process, common for all pitching motions. From Figure 6 it is seen, by inspection, that for angles of attack of about 55° to 22° in a downstroke motion, for both reduced frequencies, the values of C_N, C_D and C_m are much lower than the corresponding values for angles of attack from 22° to 55° in the upstroke motion. This difference in the flowfield during upstroke and downstroke motions is due to the lag in vortex breakdown and re-establishment process and is fully explained in [15,16,19].

For these ranges of angles of attack, $\alpha = 22°$ to 55°, the discrepancies between the experimental and predicted data are due to the abrupt changes in the slopes. For both cases examined here, i.e. interpolation ($k = 0.048$) and extrapolation ($k = 0.015$), the predicted and experimental data match exactly for the angles of attack from 0° to 22° in the upward motion and from 22° to 0° in the downward motion where there are almost no changes in the slopes. Note that for these ranges of angles of attack, $\alpha = 0°$ to 22° in the upstroke motion and $\alpha = 22°$ to 0° in the downstroke motion, Figure 6 shows that the forces and moment vary almost linearly while for the rest of the motion, $\alpha = 22°$ to 55° in the upstroke and 55° to 22° in the downstroke, variations are highly nonlinear. However, by examining Figures 6a and 6b, it is clearly seen that the differences between the measured and predicted ranges in the bifurcated range, where C_N, C_D and C_m have different values at the same angle of attack in the upward and downward motions, are within the acceptable limits.

Further note that the difference in the data at high angles of attack is caused by the flow lag and lead phenomenon. Hence, to predict these variations via neural networks, more experimental data are needed for training the network. Additional discussion about the flowfield, the vortex formation and breakdown and Reynolds number effects, as well as physical explanation regarding the effects of reduced frequency, are given in detail in [15,16,19].

The aforementioned discussion was on the 70° swept delta wing model. For the second case, a standard dynamic model, which has been tested in several wind tunnels, is considered. Figures 7 and 8 show variations of the normal force slope and pitch damping coefficients with an angle of attack for the reduced frequency of 1.5×10^{-3} and a pitching amplitude of $\alpha_A = 1°$. The aerodynamic forces and moments have been measured using a five-component internal strain gage balance. It should be noted that the present tunnel setup and the alpha-mechanism system used for changing the angle of attack of the model for both static and dynamic studies were such that the maximum static angle of attack obtainable in the test section for this particular model was about 18°. In addition, the blockage problem in dynamic tests necessitated this angle of attack limitation.

The present results are compared to the previously obtained dynamic database for this model

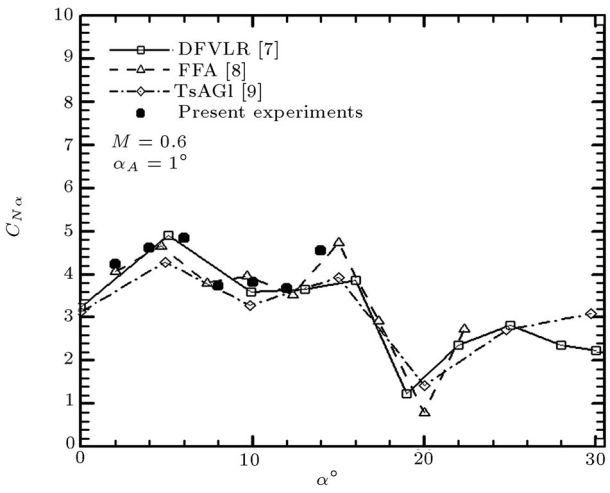

Figure 7. Variations of the slope of the dynamic normal force coefficient with angle of attack for the SDM.

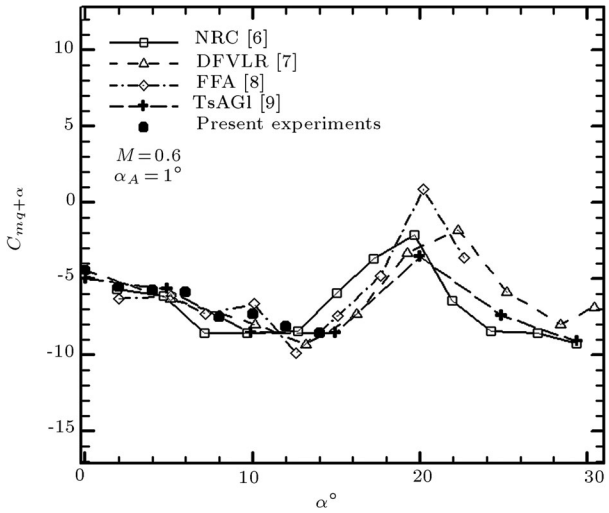

Figure 8. Variations of the pitch damping coefficient with angle of attack for the SDM.

and, as seen from Figures 7 and 8, good agreements are achieved verifying the accuracy of the measured parameters. This comparison also indicates that the experimental set up, as well as the data acquisition system, data corrections and reduction schemes, are correct. From Figure 7, note that $C_{N\alpha}$ first reaches its maximum value at about 5° angle of attack. Beyond this angle, $C_{N\alpha}$ decreases drastically indicating flow separation over the wing surface. The normal force slope continues to decrease until an angle of attack of about 10°. By further increasing the angle of attack, $C_{N\alpha}$ starts to increase again. The experimental data of [20] indicate that for a delta wing with a leading edge sweep of about 70°, the leading edge vortices start to form at an angle of attack of about 10°, causing nonlinear increase in the normal force data as shown in Figure 3. These vortices create additional lift, known as vortex lift. The present model has strakes with a leading edge sweep of about 73°. Thus, the increase in $C_{N\alpha}$, at angles of attack beyond 10°, shown in Figure 7, is due to formation of the strake vortices. From this figure it is seen that $C_{N\alpha}$ increases until an angle of attack of about 15°. This increase in $C_{N\alpha}$ is due to the strength of the strake vortices, even though the flow over the main portion of the wing is separated. Subsonic flowfield study over a wing surface of a similar model indicated that the maximum lift occurs at about a 12° angle of attack [21]. Beyond this angle of attack, the separated flow is dominated over the main portion of the wing surface, deteriorating the aerodynamic performance. As mentioned before, the present experimental setup was limited to a mean angle of attack of about 18°. However, the variations of $C_{N\alpha}$, with α for the range of angles of attack tested, compare well with those of [6-9].

Figure 8 compares variations of the present pitch damping derivative result with other findings. Again, within the range of the angles of attack tested, the data compares well with those of [6-9]. From this figure, it is seen that the pitch damping derivative continuously decreases as the angle of attack is increased, a dynamically stable condition. Beyond an angle of attack of 15°, the reduction of dynamic stability is due to the strake vortices breakdown location, which has reached the tail surfaces, hence, decreasing the stability level. For a 70° swept delta wing model, experimental data [15,20] show that the vortex burst point reaches the wing trailing edge at about 28° angle of attack. Hence, it is expected that the burst location reaches the tail surface at an angle of attack much lower than the one for the wing itself. In addition, the separated flow over the wing surface causes the strake vortices to burst at a smaller angle of attack than the one they originally would have. Therefore, the reduction in dynamic stability beyond an angle of attack of about 15° is due to the breakdown of the strake vortices, which causes flow separation over the tail surfaces and, hence, reduces their lifting mechanisms.

Figure 9 shows variations of the dynamic normal force and pitching moment coefficients with an angle of attack for three different reduced frequencies, two mean angles of attack, $\alpha_{\text{mean}} = 1^\circ$ and 5° and at a constant Mach number of 0.4. Static data for all cases are also shown for comparison. From this figure, it is seen that as the reduced frequency increases, both the slope and width of the hysteresis loops decrease. At $k = 2.2 \times 10^{-3}$, the difference between the motion of the model and flowfield around it at any instantaneous angle of attack creates the hysteresis loop in both C_N and C_m data.

From Figure 9, note that the values of C_N and C_m at any instantaneous angle of attack between upstroke and downstroke motion are different, indicating a time

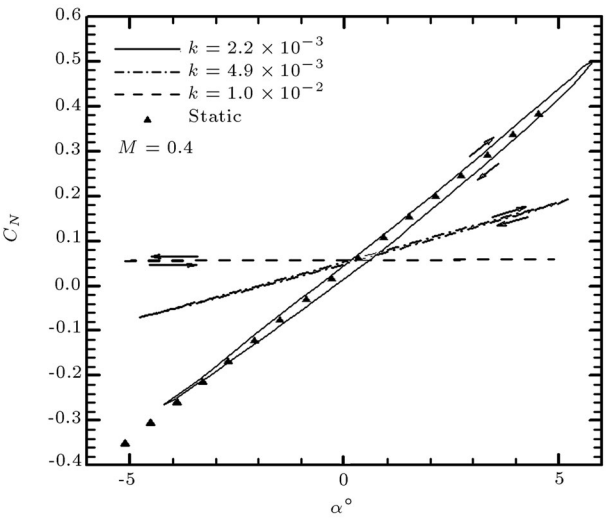

Figure 9a. Effects of the oscillation frequency on normal force coefficient for the SDM, $\alpha_{\text{mean}} = 0^\circ$.

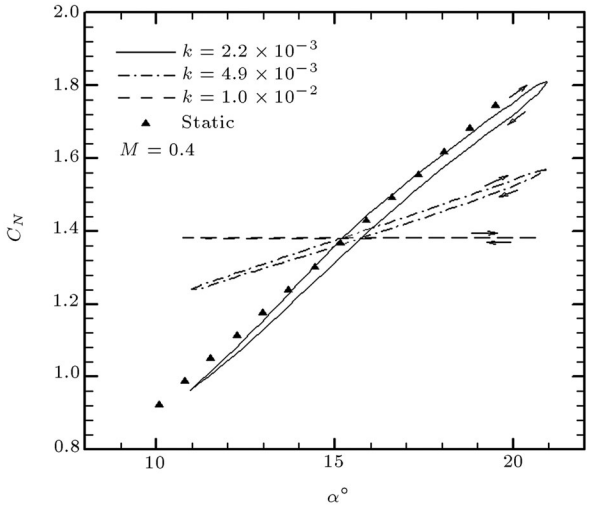

Figure 9b. Effects of the oscillation frequency on normal force coefficient for the SDM, $\alpha_{\text{mean}} = 14°$.

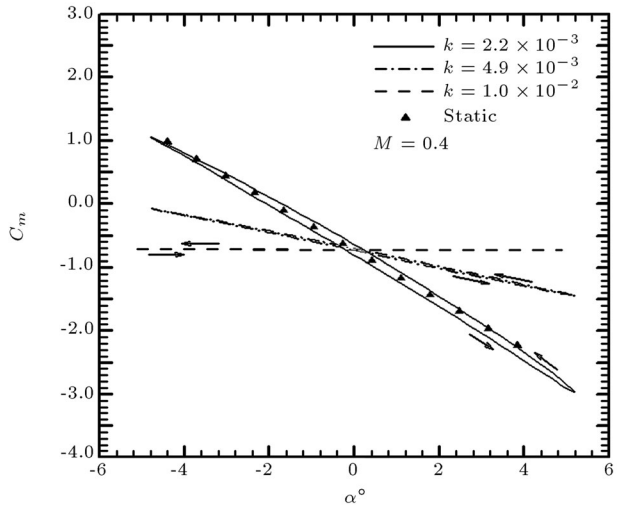

Figure 9c. Effects of the oscillation frequency on pitching moment coefficient for the SDM, $\alpha_{\text{mean}} = 0°$.

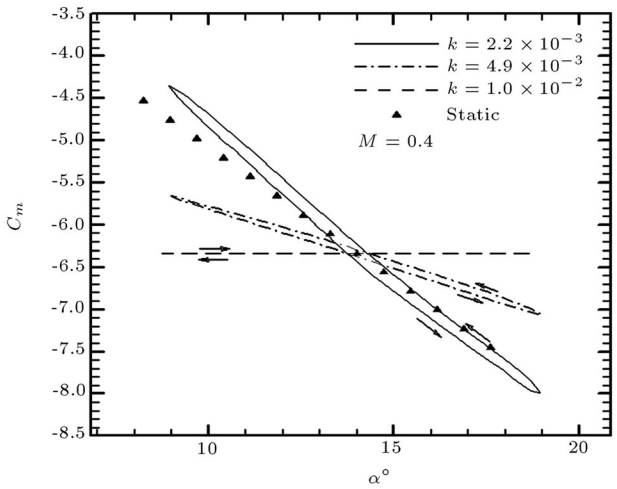

Figure 9d. Effects of the oscillation frequency on pitching moment coefficient for the SDM, $\alpha_{\text{mean}} = 14°$.

lag in the flowfield over the model. As the reduced frequency increases, the phase difference between the motion and the corresponding flow around the model decreases. Thus, the width and slope of the hysteresis loop are reduced. At $k = 0.01$, the flow no longer follows the motion of the model. Consequently, the upstroke and downstroke curves collapse on each other and C_N and C_m will have a nearly constant value for the range of angle of attack tested. Further, note that for zero° mean angle of attack, the static data for both C_N and C_m fall within the dynamic values at the reduced frequency of $k = 2.2 \times 10^{-3}$, but, for the mean angle of attack of 14°, there are some differences in static and dynamic data at $k = 2.2 \times 10^{-3}$, especially for the C_m case. This phenomenon is mainly due to the strake vortices and the effects of oscillation frequency on their development and breakdown, etc.

From this figure, the effects of mean angle of attack on the dynamic and static variation of the longitudinal force and moment of the SDM is clearly seen. As the mean angle of attack increases from 0° to 14°, the variations mentioned before become nonlinear, which is an indication of the strake vortices formation and the flow separation over the wing surface.

Using the previously trained neural network, the values of C_N were predicted for the SDM for several frequencies and mean angles of attack. Figure 10 shows variations of the mean error with σ. For the values of σ between 0.02 and 0.07, the mean error is minimum. For σ higher than 0.07, the error begins to increase slightly until, at $\sigma = 0.2$ and beyond, a drastic increase in the mean error is observed. Figure 11 shows the effects of σ on the prediction accuracy. Again, as seen from this figure, σ has a pronounced effect on predicting C_N. For all test cases examined here, a value of $\sigma = 0.03$ gives minimum error. Thus, for this model throughout the

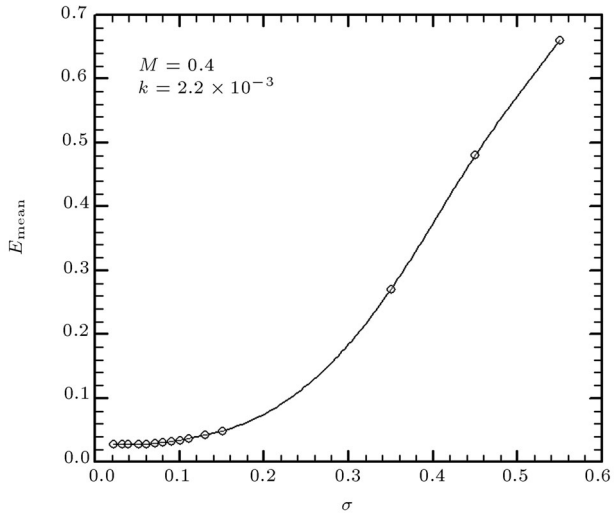

Figure 10. Effects of σ on the mean error prediction for the SDM.

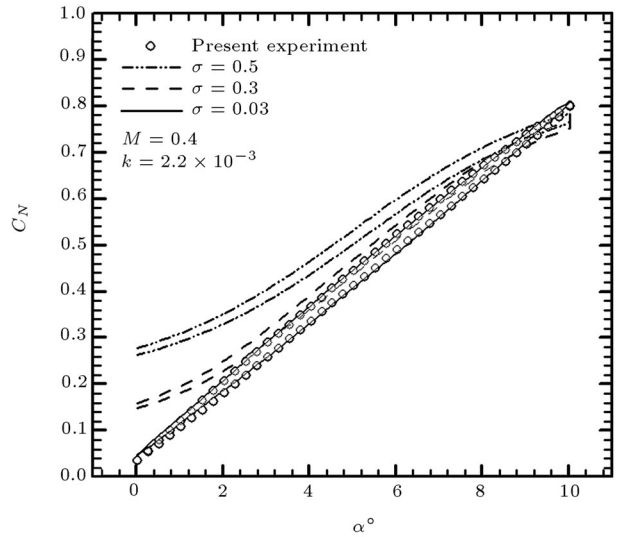

Figure 11. Effects of σ on predicting the normal force coefficient for the SDM.

paper, the value of $\sigma = 0.03$ has been chosen as the optimum σ.

Figure 12 shows variations of the normal force coefficient with angles of attack for four typical cases of $\alpha_{\text{mean}} = 0^\circ, 4^\circ, 6^\circ$ and 10°. Note that for all cases considered in this figure, the value of the free stream Mach number was 0.4 and the reduced frequency was 2.2×10^{-3}. The experimental data for each case is compared with the GRNN predicted data. Again, the predicted data for each case is the result of the extrapolation or interpolation of the experimental data. The experimental data were obtained at the mean angles of attack of 0° to 14°.

For each case presented in Figure 12, the GRNN has been trained such that it's output is either extrapolating or interpolating the experimental data. For

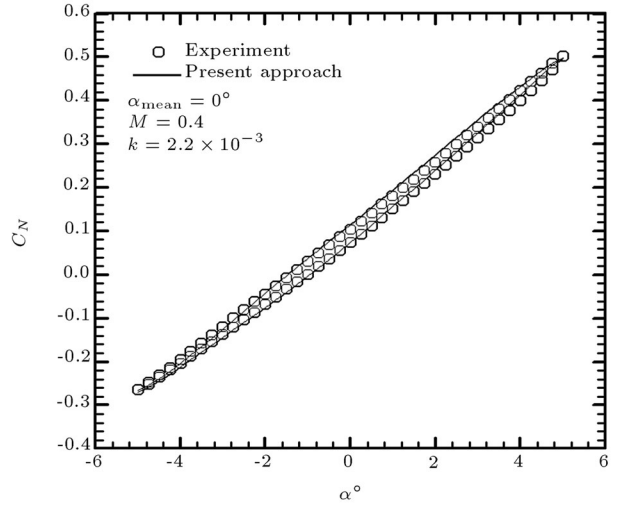

Figure 12a. Comparison of the predicted and experimental normal force coefficient data for the SDM, $\alpha_{\text{mean}} = 0^\circ$, $k = 2.2 \times 10^{-3}$.

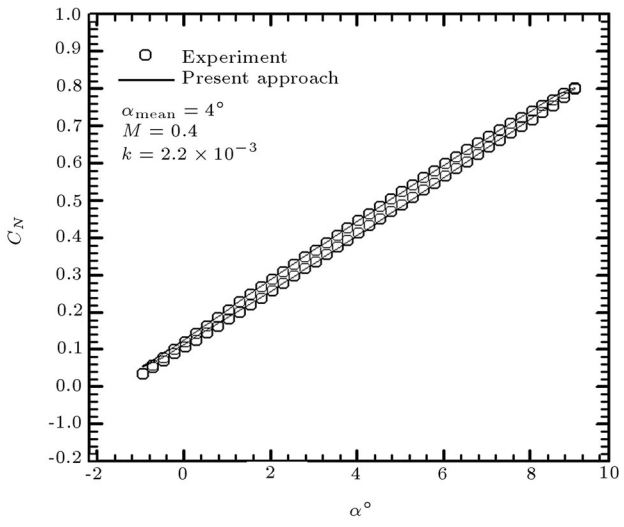

Figure 12b. Comparison of the predicted and experimental normal force coefficient data for the SDM, $\alpha_{\text{mean}} = 4^\circ$, $k = 2.2 \times 10^{-3}$.

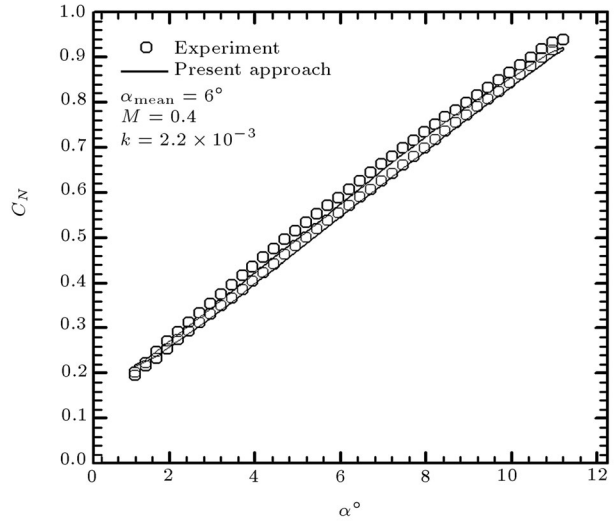

Figure 12c. Comparison of the predicted and experimental normal force coefficient data for the SDM, $\alpha_{\text{mean}} = 6^\circ$, $k = 2.2 \times 10^{-3}$.

instance, in Figure 12a, the GRNN was trained using the experimental variations of C_N with angle of attack for the mean angles of 2°, 4°, 6° and 8°, while its output is for the mean angle of attack of 0°, that is, extrapolating the experimental data. For Figure 12b the trained experimental data were for $\alpha_{\text{mean}} = 0^\circ$, 2°, 6° and 8° and the GRNN has interpolated the acquired data for the mean angle of 4°.

From this figure, it is seen that the prediction accuracy is sufficiently high at low mean angles of attack (Figures 12a and 12b). However, as the mean angle increases, some discrepancies are observed between the predicted and experimental data. Comparing Figures 12c and 12d with 12a and 12b, it is clearly seen that for mean angles of attack of $\alpha_{\text{mean}} = 6^\circ$ and

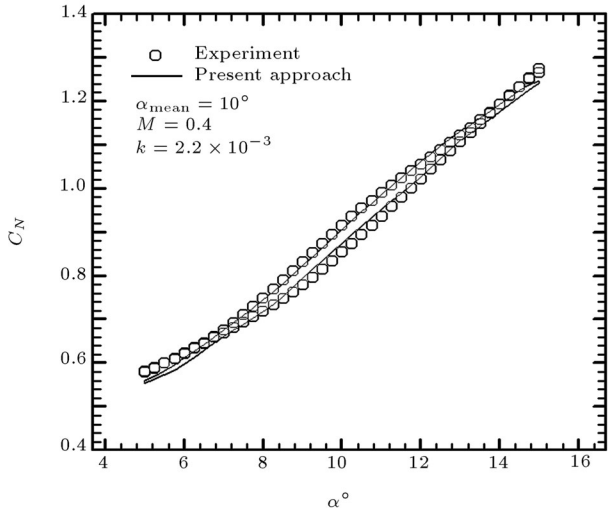

Figure 12d. Comparison of the predicted and experimental normal force coefficient data for the SDM, $\alpha_{mean} = 10°$, $k = 2.2 \times 10^{-3}$.

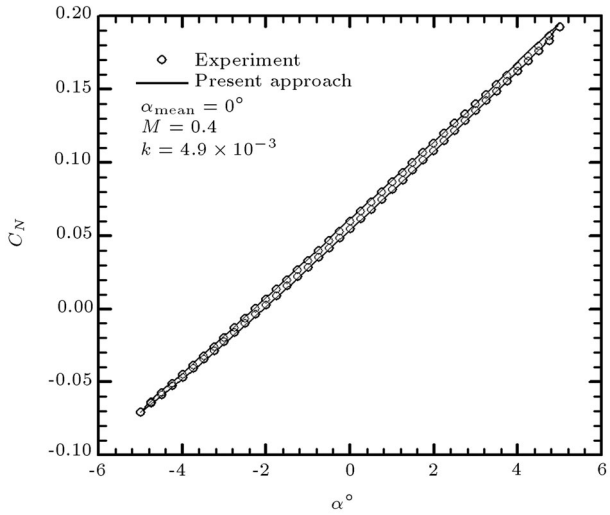

Figure 13a. Comparison of the predicted and experimental normal force coefficient data for the SDM, $\alpha_{mean} = 0°$, $k = 4.9 \times 10^{-3}$.

10°, the shape of the hysteresis loop is slightly different from that of the lower mean angles, i.e., $\alpha_{mean} = 0°$ and 4° (Figures 12a and 12b). These differences are caused by the strake vortex formation and breakdown over the tail surface and the wing flowfield, as discussed previously.

Furthermore, comparing Figure 12c with 12d, it is clearly seen that the network has been able to predict the variation of C_N with angle of attack for the mean angle of 6° much better than that of 10° (Figure 12d). The maximum angle of attack from Figure 12d was 15°, hence, it is likely that the flow re-attachment process in the downstroke motion is delayed, due to fast variations of the angle of attack, thus, differing the shape of the hysteresis loop when compared with other cases. For the mean angles of attack of 0° and 4°, the small hysteresis in experimental data between increasing and decreasing the angle of attack is caused by the dynamic effects rather than the flowfield variations over different parts of the model. Since, for these angles of attack, the flow over the main portion of the model is attached, thus, as expected, the deviations between the aerodynamic loads in upstroke and downstroke motions are minimal.

Figure 13 shows both the predicted and experimental variations of the normal force coefficient with angles of attack for two different mean angles of attack of $\alpha_{mean} = 0$ and 10° and a reduced frequency of 4.9×10^{-3} at a constant Mach number of 0.4. It can be seen that the predicted data compare well with the measured ones, verifying the accuracy and capability of the proposed approach. The results for other cases, i.e., different mean angles of attack, reduced frequencies and Mach numbers show similar trends and are not included in this paper.

For the highest reduced frequency examined here,

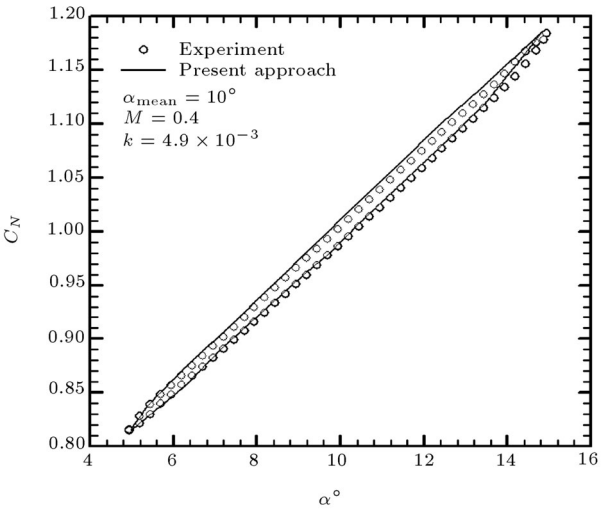

Figure 13b. Comparison of the predicted and experimental normal force coefficient data for the SDM, $\alpha_{mean} = 10°$, $k = 4.9 \times 10^{-3}$.

$k = 0.01$, for all combinations of mean angles of attack and Mach numbers, the present experimental data show that variations of the aerodynamic force and moment with angle of attack is almost constant with no hysteresis loop in the data (see Figure 9). Therefore, the GRNN was not trained for this reduced frequency.

The pitching moment from the balance data in the present experiments is obtained using the normal forces measured at the forward and aft strain gauges in the balance, hence, its variation is similar to that of the normal force, as seen in Figure 9. Thus, the pitching moment data for the cases beyond those tested in the tunnel, were not predicted via the GRNN method. However, the method is similar and the GRNN can easily predict variations of the pitching moment with

angles of attack for various Mach numbers, mean angles of attack, reduced frequencies, etc. as was done for the normal force, even though it has not been shown in this paper.

CONCLUSION

A new method based on the Generalized Regression Neural Network has been introduced to predict unsteady aerodynamic forces and moment on vehicles undergoing sinusoidal pitching motion. Extensive wind tunnel tests have been conducted on two different models to train the network and check its prediction accuracy. For the delta wing model, the GRNN predictions of C_N, C_D and C_m data for various cases are shown to be accurate enough, except for the regions where there was an abrupt change in the force or moment coefficients, i.e. bifurcation region. The aerodynamic behavior of the SDM was slightly different. The wing sweep for this model was about 40° and the experiments were restricted to mean angles of attack of about 15°. Therefore, the shape of the hysteresis loops for all cases examined, were nearly ellipsoid.

However, the same network could successfully predict the normal force coefficient of this model. The output results of the network were in good agreement with those obtained in the wind tunnel. At angles of attack where some complicated phenomena were caused by flow separation over the wing surface and the strake vortex formation and breakdown, there are some deviations between the values predicted by the GRNN and the experimental data, thus, the network must be trained with more data points in those regions. Further work, including the effects of Mach number and reduced frequency, etc. is underway to improve and extend the capability of the proposed method.

ACKNOWLEDGMENT

The authors would like to express their sincere thanks to the Iranian AIO, especially the Vice Chairman of the Training and Research Department, for funding this research program. In addition, the support of the Qhadr research center personnel in conducting the tests and acquiring the data is deeply appreciated.

NOMENCLATURE

U	free stream velocity, m/sec
M	free stream Mach number
f	oscillation frequency, Hz
S_{ref}	wing area, m^2
c	wing mean aerodynamic chord, m
$\text{Re} = U/\nu$	Reynolds number,/m
$\omega = 2\pi f$	angular velocity, rad/sec
$k = c\omega/2U$	reduced frequency
α	instantaneous angle of attack, deg.
α_A	oscillation amplitude, deg.
α_{mean}	oscillation mean angle of attack, deg.
C_L	lift coefficient
C_N	normal force coefficient
C_m	pitching moment coefficient
$C_{N\alpha}$	dynamic normal force slope, /rad
$C_{m_{q+\alpha}}$	pitch damping derivative, /rad
σ	the correlation parameter in the generalized regression neural network
E_{mean}	the mean squared error between the actual and predicted samples

REFERENCES

1. La Marsh, W.J., Walsh, J.L. and Rogers, J.L. "Aerodynamic performance optimization of a rotor blade using a neural network as the analysis", *AIAA*, pp 92-4837 (Sept. 1992).
2. McMiller, R.L., Steck, J.E. and Roshaz, K. "Application of an artificial neural network as a flight test data estimator", *Journal of Aircraft*, **32**(5) (1995).
3. Faller, W.E. and Schreck, S.J. "Real time prediction of unsteady aerodynamics: Application of aircraft control and maneuverability enhancement", *IEEE Transactions on Neural Networks*, **6**(6) (1995).
4. Lo, C.F. and Zhao, J.L. "Application of neural networks to wind tunnel data response surface methods", *AIAA*, pp 2000-2639 (June 2000).
5. Berdahl, C. "Neural network detection of shockwaves", *AIAA Journal*, **40**(3) (March 2002).
6. Beyers, M.E. "SDM pitch and yaw axis stability derivatives", *AIAA*, pp 85-1827 (1985).
7. Schmidt, E. "Standard dynamics model experiments with the DFVLR/AVA transonic derivative balance", *AGARD CP-386* (May 1985).
8. Jansson, T. and Torngren, L. "New dynamic testing techniques and related results at FFA", *AGARD CP-386* (May 1985).
9. Khrabrov, A.N., Private Communications.
10. Specht, D.F. "A general regression neural network", *IEEE Trans. on Neural Networks*, **2**(6), pp 568-576 (1991).
11. Parzen, F. "On estimation of a probability density function and mode", *Ann. Math. Statist.*, **33**, pp 1065-1076 (1962).
12. Cacoullos, T. "Estimation of a multivariable density", *Ann. Math. Statist.*, **18**(2), pp 179-189 (1966).
13. Kung, S.Y., *Digital Neural Network*, Prentice-Hall Inc., pp 29-34 (1993).

14. Soltani, M.R., Sadati, N. and Davari, A.R. "Neural network: A new prediction tool for estimating the aerodynamic behavior of a pitching delta wing", *AIAA*, pp 2003-3793 (2003).

15. Soltani, M.R. "An experimental study of the relationship between forces and moments and vortex breakdown on a pitching delta wing", Ph.D. Thesis, Department of Aeronautical Engineering, University of Illinois at Urbana-Champaign, USA (1992).

16. Soltani, M.R., Bragg, M.B. and Brandon, J.M. "Measurements on an oscillating 70° delta wing in subsonic flow", *Journal of Aircraft*, **27**(3) (March 1990).

17. Polhamus, E.C. "Prediction of vortex-lift characteristics by leading-edge suction analogy", *Journal of Aircraft*, **8**(4), pp 193-199 (1971).

18. Hummel, D. and Srinivasan, P.S. "Vortex break down effects on the low speed aerodynamic characteristics of slender delta wings in symmetrical flow", *Journal of the Royal Aeronautical Society*, **71**, pp 319-322 (1967).

19. Soltani, M.R., Ebrahimi, S.A. and Davari, A.R. "A new method for predicting the amplitude and frequency of a highly swept wing undergoing rocking motion", *International Journal of Science and Technology, Scientia Iranica*, **10**(2), pp 175-185 (2002).

20. Wentz, W.H. "Wind tunnel investigations of vortex break downs", Ph.D. Dissertation, University of Kansas, Lawrence, KS, USA (1968).

21. Soltani, M.R., Khadivi, T. and Abbasi, A. "Flowfield study over the wing of a fighter model", *International Journal of Engineering, Trans B: Application*, **16**(4), pp 405-416 (Dec. 2004).